Talanta 83 (2010) 241–248

Contents lists available at ScienceDirect

Talanta

journal homepage: www.elsevier.com/locate/talanta

Niobium oxide dispersed on a carbon–ceramic matrix, $SiO_2/C/Nb_2O_5$, used as an electrochemical ascorbic acid sensor

Leliz T. Arenas[a], Paulo C.M. Villis[a], Jacqueline Arguello[b], Richard Landers[c], Edilson V. Benvenutti[b], Yoshitaka Gushikem[a,*]

[a] Institute of Chemistry, State University of Campinas, Inorganic Chemistry, Campinas, SP, Brazil
[b] Institute of Chemistry, Federal University of Rio Grande do Sul, Porto Alegre, RS, Brazil
[c] Institute of Physics Gleb Wataghin, State University of Campinas, Campinas, SP, Brazil

ARTICLE INFO

Article history:
Received 10 May 2010
Received in revised form 8 September 2010
Accepted 8 September 2010
Available online 16 September 2010

Keywords:
Silica niobia composite
Carbon–ceramic electrode
Vitamin C sensor
Sol–gel

ABSTRACT

A film of niobium oxide was immobilized on a SiO_2/C carbon–ceramic matrix (specific surface area 270 $m^2\ g^{-1}$) and characterized by N_2 adsorption–desorption isotherms, scanning electron microscopy, X-ray photoelectron spectroscopy and atomic force microscopy. This new carbon–ceramic material, $SiO_2/C/Nb_2O_5$, was used for construction of electrodes, and it shows ability to improve the electron-transfer between the electrode surface and ascorbic acid. The electrocatalytic oxidation of ascorbic acid was made by differential pulse and cyclic voltammetry techniques, making it potentially useful for developing a new ascorbic acid sensor.

1. Introduction

Due to physical and chemical properties such as high refractive index, wide band gap, chemical stability and corrosion resistance, Nb_2O_5 films dispersed on porous solid matrices have been widely used as optical and electronic devices [1,2], catalysts [3–7], and ion exchange materials [8,9]. Among the porous solid matrices that serve as supports, silica has attracted attention because the deposition of Nb_2O_5 on the surface occurs by formation of Si–O–Nb bonds, forming a thermally very stable thin film [10]. Additionally, Nb_2O_5 is known for its affinity to adsorb species containing the carboxylic acid group, and it has been proposed as a potential interface for the immobilization of organic molecules and biomolecules to be applied in the development of electrochemical sensors [10–14].

The development of silica based carbon–ceramic electrodes (CCEs) is now a wide field of investigation. These electrodes present the mechanical rigidity of the inorganic framework and the conductivity of graphite; furthermore they have a wide operational voltage window and present renewable surfaces, making possible their use in electroanalysis and electrocatalysis [15–19]. Recently it was reported the use of carbon–ceramic electrodes for detection of organic species such dopamine, uric acid and ascorbic acid [20].

Ascorbic acid (H_2AA) is one of the most important water soluble components present in fruits and vegetables. H_2AA is used in large scale as an antioxidant in food, animal feed, beverages, pharmaceutical formulations and cosmetic applications. Because of its biological and technological importance, the development of electrochemical sensors for H_2AA has received a great attention in the last years, where the search for new materials that can improve the electrochemical analyses has been enhanced [21–26].

In this work, Nb_2O_5 film was immobilized by a grafting reaction on a carbon–ceramic matrix obtained by the sol–gel method. The material $SiO_2/C/Nb_2O_5$ was characterized using N_2 adsorption–desorption isotherms, scanning electron microscopy, X-ray photoelectron spectroscopy and atomic force microscopy techniques. Differential pulse voltammetry (DPV) and cyclic voltammetry (CV) were employed to study the electrochemical behaviour of this electrode in the oxidation of ascorbic acid, H_2AA.

2. Experimental

2.1. Preparation of the carbon–ceramic SiO_2/C

The carbon–ceramic matrix was prepared by the sol–gel method according to the following procedure: 0.11 mmol of TEOS (tetraethylorthosilicate, Acros 98%), was hydrolyzed in a mixture of 25 mL of ethanol, 4.0 mL of water and 0.86 mL of 37% HCl. After vigorous stirring at 343 K for 4 h, 3.3 g of graphite powder (99.99% Aldrich) was then added and the mixture was ultrasonicated for

* Corresponding author. Tel.: +55 19 3521 3053; fax: +55 19 3521 3023.
E-mail address: gushikem@iqm.unicamp.br (Y. Gushikem).

0039-9140/$ – see front matter © 2010 Elsevier B.V. All rights reserved.
doi:10.1016/j.talanta.2010.09.014

20 min. To this mixture 4.0 mL of water was added and ultrasonicated at 333 K until gelation of the material occurred. It was then allowed to stand for 5 days at 313 K for solvent evaporation. This xerogel was comminuted to a fine powder and then washed with ethanol in a Soxhlet extractor for 6 h. Finally, the xerogel was dried under vacuum (1.0×10^{-2} kPa) at 340 K during 4 h.

2.2. Nb_2O_5 immobilization on SiO_2/C

To prepare the starting solution for deposition of niobium oxide on SiO_2/C, initially 1.9 g of $NbCl_5$ was dissolved in 80 mL of dry ethanol under a nitrogen atmosphere and gently shaken for 24 h to eliminate gaseous HCl. The following reaction may take place during solution preparation [27].

$$NbCl_5 + nHOC_2H_5 \rightarrow Nb(OC_2H_5)_nCl_{5-n} + nHCl(\text{solutionA})$$

Separately, about 20 mg of the dried and powdered SiO_2/C was pressed under 4 ton pressure in a disk format with diameter of 5 mm and a thickness of 1 mm. On the clean disk surface of SiO_2/C a drop of a solution A (0.05 mL) was spread on the disk surface (Scheme 1B) and then exposed to room wet atmosphere for 30 min to eliminate the ethanol and remaining HCl (Scheme 1C). The disk was then washed with water and heated at 353 K for 3 h for drying and consolidation of the Nb_2O_5 on the SiO_2/C surface (Scheme 1D).

2.3. N_2 adsorption–desorption isotherms

The nitrogen adsorption–desorption isotherms of the SiO_2/C xerogel previously degassed at 423 K, were determined at the liquid nitrogen boiling point on a Quantachrome Autosorb 1 Instrument. The specific surface area was determined from the BET (Brunauer, Emmett and Teller) multipoint method [28]. The pore size distribution was obtained using the BJH (Barret, Joyner, and Halenda) method [29].

2.4. Scanning electron microscopy (SEM)

SEM images were obtained using a JEOL JSM 6360LV scanning electron microscope connected to a secondary electron detector with energy dispersive X-ray spectroscopy (EDS) for elemental mapping. The micrograph was obtained with a magnification of 1200× operating at an accelerating voltage of 20 kV. The sample was dispersed on double faced conducting tape on an aluminum support and carbon-coated in a Bal-Tec MD20 instrument.

2.5. Electrical properties

Solid state electrical conductivities of the SiO_2/C and SiO_2/C/Nb_2O_5 disks were calculated by the equation: $\sigma = \rho^{-1}$, where σ is the conductivity and ρ is the resistivity. The ρ was obtained according to a procedure described elsewhere [30], assuming that the graphite and Nb_2O_5 were dispersed on a non-conductor substrate, and calculated by the equation $\rho = R\, w\, F_2\, F_4$, where R is the electrical resistance, w is the thickness of the disk (0.10 cm), F_2 and F_4 are correction factors which were taken from the literature (0.5 and 0.9816 respectively) [30]. The R values of the samples were measured at room temperature using a National Instruments NIPXI-1033 four-point probe.

2.6. X-ray photoelectron spectroscopy

The X-ray photoelectron (XPS) spectra of the samples were obtained by using an aluminum anode (Al K = 1486.6 eV) at a pressure of 2.63×10^{-5} Pa on a McPherson ESCA-36 spectrometer. The binding energies were calibrated against the Si 2p level (103.5 eV)

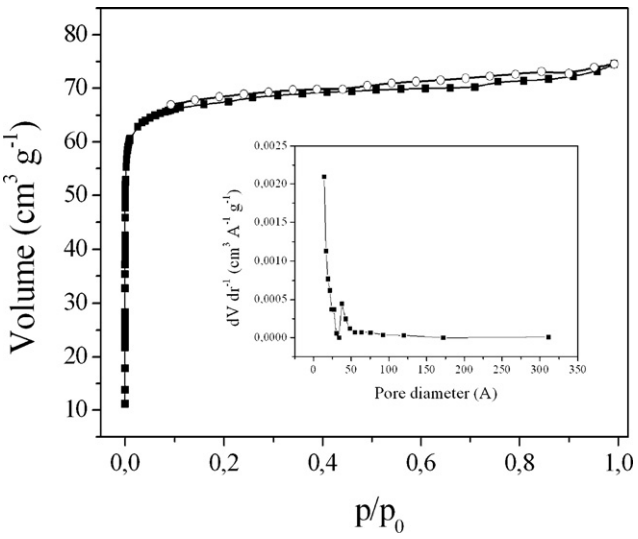

Fig. 1. N_2 adsorption–desorption isotherms of SiO_2/C. Inset figure: the respective BJH pore size distribution.

2.7. Atomic force microscopy (AFM/EFM)

AFM/EFM measurements were carried out on a Nanoscope IIIa (Digital Instruments) apparatus at room temperature. The surface topography was determined with the tapping mode. Upon retrace over the same line, the electrical force was monitored under a non-contact mode at a set lift height of 200 nm from the sample surface. A dc bias voltage of 3 V was applied between across the tip and the sample

2.8. Electrochemical study

Electrochemical measurements were carried out using a PGSTAT-20 Autolab potentiostat–galvanostat with GPES software for collection and analysis of data. A three-electrode system was used, including a saturated calomel electrode (SCE) as reference electrode, a platinum wire as counter electrode and a SiO_2/C or SiO_2/C/Nb_2O_5 disk as working electrode. The disks were glued to a glass tube with glue and the electrical contact was made by a copper wire inserted inside the glass tube. In order to improve the connection between the metal and the disk surface, pure graphite powder was added to the tube. The electrolyte solution was 0.5 mol L^{-1} KCl in a 0.1 mol L^{-1} Tris–HCl buffer. Experiments were conducted at room temperature under a nitrogen atmosphere.

3. Results and discussion

3.1. Characterization

3.1.1. Specific surface area and pore size distribution

The SiO_2/C ceramic prepared by the sol–gel method resulted in a porous material with a specific surface area of 270 $m^2\, g^{-1}$ and pore volume of 0.07 $cm^3\, g^{-1}$. N_2 adsorption isotherm obtained for this material shows a type I curve (Fig. 1), typical of microporous material [31]. Pores with diameters lower than 20 Å were observed in the pore size distribution curve obtained from BJH method (inset Fig. 1).

3.1.2. Micrograph

Fig. 2 illustrates the backscattering SEM image of the disk surface of SiO_2/C immobilized with Nb_2O_5 oxide film and the corresponding C, Si, and Nb EDS mapping images. Two different distribution areas are seen: light-gray and dark-gray zones. In the mapping

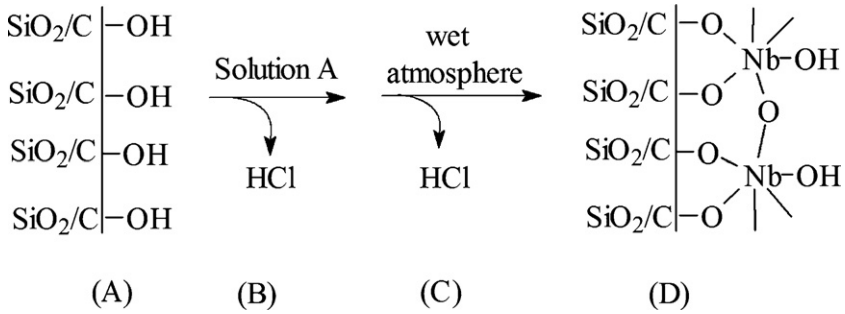

Scheme 1. (A) Pressed SiO_2/C disk; deposition of Nb(V) on pressed SiO_2/C disk; (B) reaction with $Nb(OC_2H_5)_nCl_{5-n}$; (C) exposition to wet atmosphere and (D) the modified $SiO_2/C/Nb_2O_5$ disk.

images these zones correspond to silica and carbon particles, respectively. In the niobium mapping images, the Nb_2O_5 particles are uniformly dispersed on the disk surface, at the sub micrometric level, considering the magnification used.

3.1.3. X-ray photoelectron spectroscopy (XPS)

To determine the chemical state of the components, the surface of the $SiO_2/C/Nb_2O_5$ material was analyzed by XPS. Fig. 3 shows the XPS spectra and the respective deconvolution curves of the C 1s, O 1s, Si 2p, and Nb 3d core levels. The XPS binding energy values (BE), full-width at half maximum of the peaks, the areas under peaks, and atomic percentages of the elements are summarized in Table 1.

The broad asymmetrical C 1s peak (Fig. 3(a)), consists of four contributions related to the graphitic structure. The main peak is detected at 284.2 eV and attributed to the carbon of the planar graphite network [32]. The other contributions located at 285.8, 287.6 and 289.9 eV corresponding to oxidized graphite [33–35], C–OH, C–O–C and COOH, respectively. In the O 1s deconvoluted spectrum (Fig. 3(d)) three peaks with different binding energies appear, indicating that oxygen atoms are involved in three distinct chemical bonds. The peaks located at 530.3 and 532.4 eV correspond to O–Nb and O–Si, respectively, [36,37] and the third peak centered at 534.3 eV could be attributed to the O–C bond on the oxidized graphite surface.

The Si 2p spectra (Fig. 3(b)) show a peak at 103.3 eV assigned to silicon in Si–O, Si–OH and Si–O–Si bonds and the other peak at 105.8 eV due to the protonated oxide surface, $Si–OH_2^+$ [38]. In the Nb spectrum (Fig. 3(c)), the Nb $3d_{5/2}$ and Nb $3d_{3/2}$ peaks are observed at 207.4 and 210.1 eV, respectively. These values match those obtained for niobium oxide [36,39], evidencing the formation of the Nb_2O_5 film on the SiO_2/C surface. The Nb/Si atomic ratio obtained by XPS was 1.61.

3.1.4. Atomic force microscopy

The $SiO_2/C/Nb_2O_5$ surface was examined by AFM/EFM, and the images are shown in Fig. 4. Significant changes in contrast are observed before (a) and after film formation (b), the smoother appearance originated by the presence

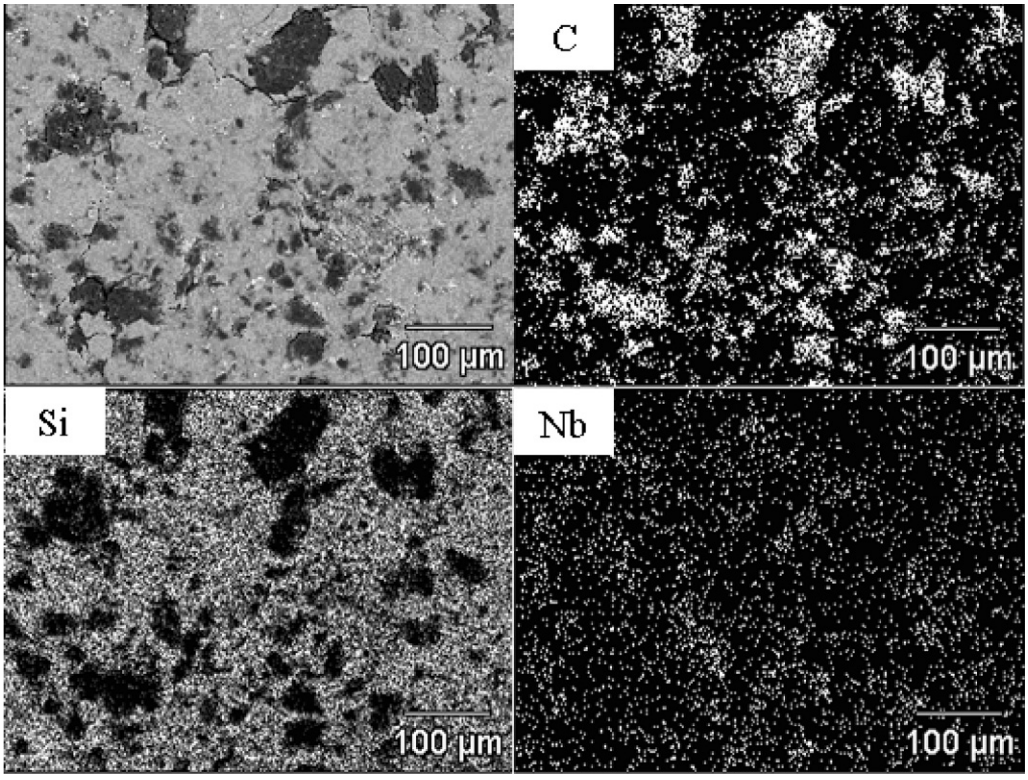

Fig. 2. SEM image of $SiO_2/C/Nb_2O_5$, and the corresponding EDS mapping of C, Si and Nb. The magnification was 200×.

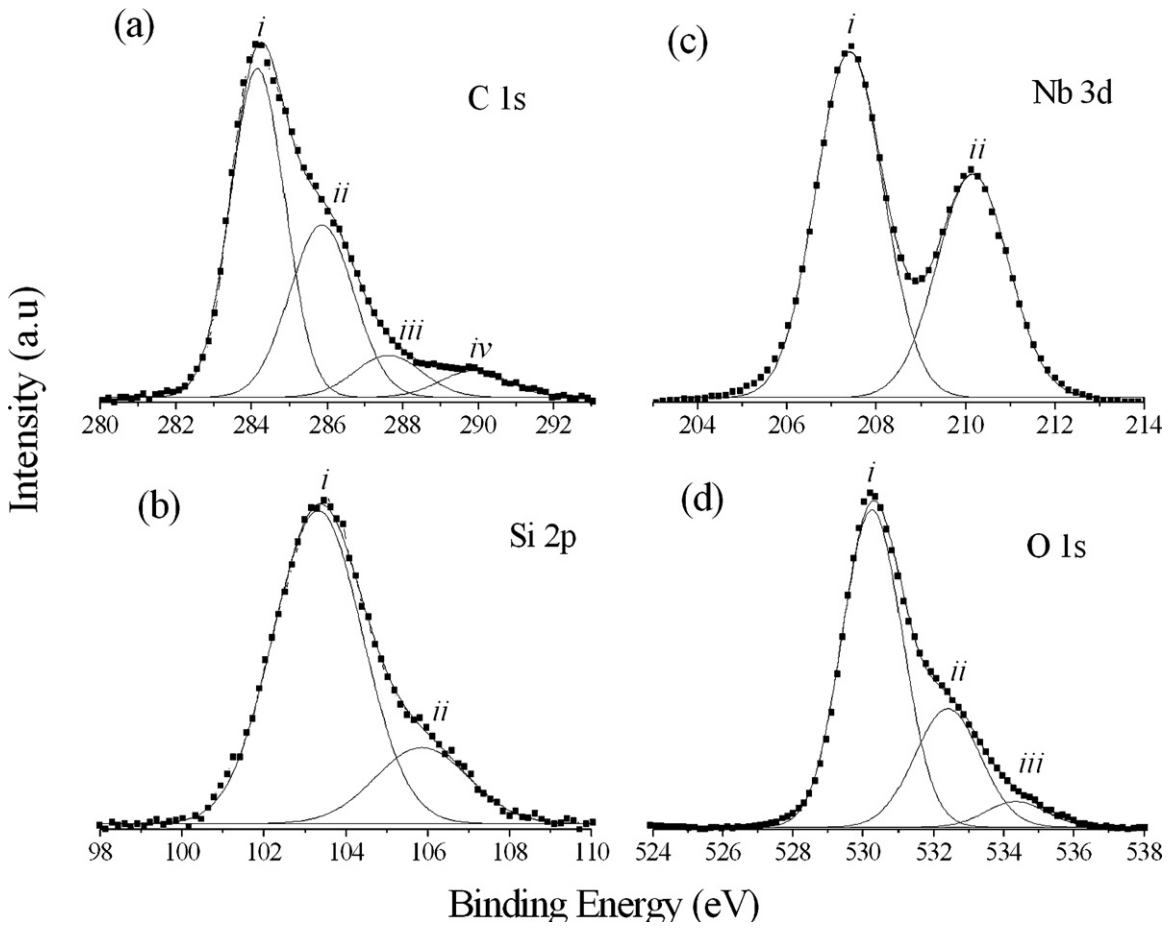

Fig. 3. X-ray photoelectron spectra of the C 1s (a), Si 2p (b), Nb 3d (c) and O 1s (d) regions for the $SiO_2/C/Nb_2O_5$.

of niobium oxide demonstrated its ability to improve the conductivity of the electrode by facilitating a more uniform charge of distribution on the carbon–ceramic material.

3.1.5. Conductivity of the pressed disk

Electrical conductivity measurement of the pure carbon–ceramic matrix SiO_2/C shows $0.9 \pm 0.3\,S\,cm^{-2}$, indicating that graphite particles are well dispersed and interconnected in the silica network, as seen by the SEM image. However, after the deposition of the Nb_2O_5 film, the conductivity increased to $1.5 \pm 0.3\,S\,cm^{-2}$. This increase is evidence that the oxide presence improves the conductivity of the solid.

3.2. Electrochemical characterization and electrocatalytic properties

Potassium ferrocyanide and potassium ferricyanide solutions ($1\,mmol\,L^{-1}$) were employed as redox probe for characterization of $SiO_2/C/Nb_2O_5$ by cyclic voltammetry at a scan rate of $40\,mV\,s^{-1}$. A peak potential separation (ΔEp) of 78 mV was observed indicating a quasireversible redox process. The active area of the electrode was estimated by applying the Randles–Sevcik equation as described in the literature [40] and $0.26\,cm^{-2}$ was found.

The electrocatalytic activity of the $SiO_2/Nb_2O_5/C$ electrode in the oxidation of ascorbic acid (H_2AA) was studied. Fig. 5 shows the differential pulse voltammograms (DPV) of $1.0 \times 10^{-3}\,mol\,L^{-1}$ of H_2AA on the SiO_2/C electrode (Fig. 5(a)) and on the $SiO_2/C/Nb_2O_5$

Table 1
XPS data for $SiO_2/C/Nb_2O_5$ disk.

	Binding energies (eV)									
	C 1s				O 1s			Si 2p		Nb 3d
	i	*ii*	*iii*	*iv*	*i*	*ii*	*iii*	*i*	*ii*	
$SiO_2/Nb_2O_5/C$	284.2	285.8	287.6	289.9	530.3	532.4	534.3	103.3	105.8	207.4
	(1.7)[a]	(2.0)	(2.1)	(2.1)	(2.0)	(2.0)	(2.0)	(2.5)	(2.5)	(1.8)
	[53][b]	[33]	[9]	[5]	[67]	[28]	[5]	[80]	[20]	
	{46.3}[c]				{36.3}			{6.6}		{10.8}
SiO_2[d]					532.5			103.3		
Nb_2O_5[e]					530.4					207.4

[a] Full-width at half maximum of the peaks.
[b] Relative areas of the peaks.
[c] Relative atomic relative percentages.
[d] BE reference data for SiO_2 [25].
[e] BE reference data for Nb_2O_5 [25].

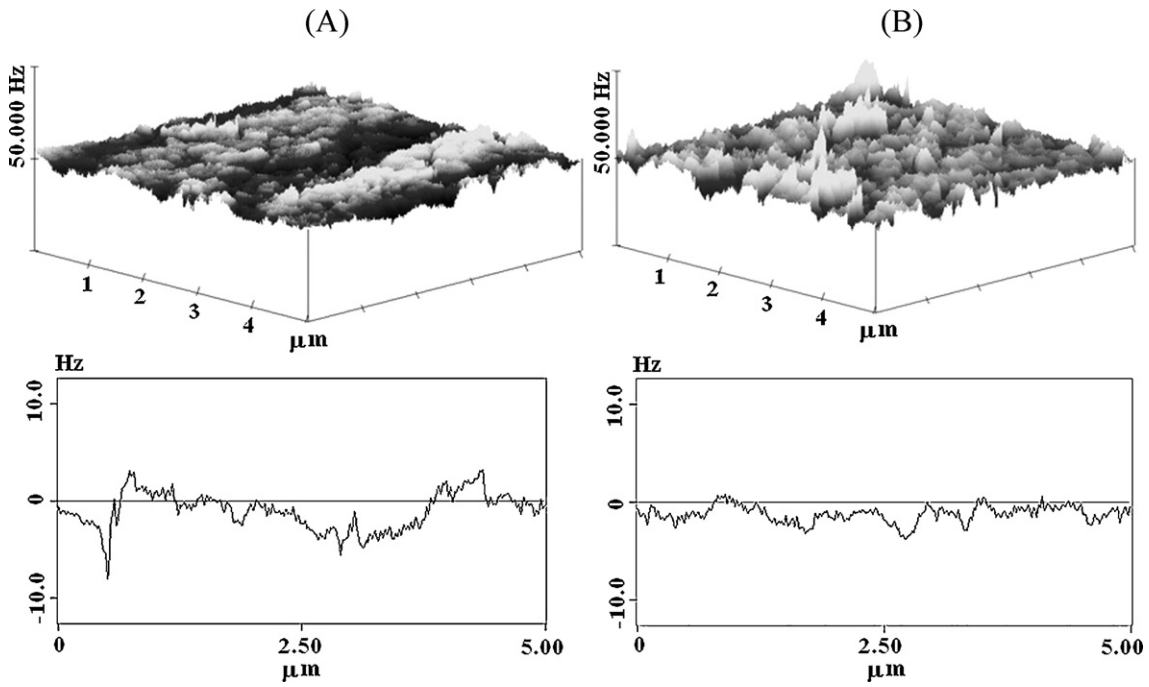

Fig. 4. 3D EFM images (5 μm × 5 μm × 25 Hz) of (a) carbon–ceramic SiO_2/C and (b) SiO_2/C/Nb_2O_5, and the respective horizontal cross section analysis taken at the middle of the image.

electrode (Fig. 5(b)). It can be seen that the presence of Nb_2O_5 at the SiO_2/C surface reduces the overvoltage of H_2AA oxidation, shifting the potential of oxidation to a value more negative by about 0.18 V. The peak current is considerably enhanced compared with the response of H_2AA on the SiO_2/C electrode surface. This behaviour clearly demonstrates the electrocatalytic function of the SiO_2/C/Nb_2O_5 electrode toward ascorbic acid oxidation.

The voltammetric response of H_2AA on the SiO_2/C/Nb_2O_5 electrode may be ascribed to the interaction between the Nb_2O_5 and H_2AA. The interaction includes the formation of covalent bonds between the niobium oxide and H_2AA [41], as shown in Scheme 2, which might lead to a very fast kinetics of H_2AA oxidation on the SiO_2/C/Nb_2O_5 surface. Moreover, niobium oxide is an n-type semiconductor; the conduction band is built from the 3d orbital of the Nb atoms and the valence band from the 2p orbitals of oxygen [42], it is certain that the electrical conductivity at potentials above the conduction band edge may facilitate transfer of electrons in the oxidation of H_2AA. Scheme 2 shows the possible reaction mechanism, where H_2AA is initially adsorbed on the electrode surface by formation of covalent bond with the niobium oxide, and then oxidized to dehydro ascorbate involving two electrons and two protons [43].

The cyclic voltammograms of SiO_2/C/Nb_2O_5 at various scan rates (10–100 mV s^{-1}) in the presence of 2.0×10^{-3} mol L^{-1} of H_2AA was studied (Fig. 6(a)). The oxidation current, *ip* (anodic peak current), for H_2AA increased linearly with the scan rate (Fig. 6(b)), according to the equations $ip\ (\mu A) = (2.05 \pm 0.01)\nu\ (mV s^{-1}) + (17.68 \pm 1.02)$, with a linear correlation, $r = 0.999$, confirming an adsorption-controlled process. In addition, there is a linear relation between $\log ip$ and $\log \nu$, corresponding to the following equation: $\log ipa = (0.71 \pm 0.02) + (0.82 \pm 0.012)\log \nu$; $r = 0.991$. The slope value of 0.82 may be considered as closed to the

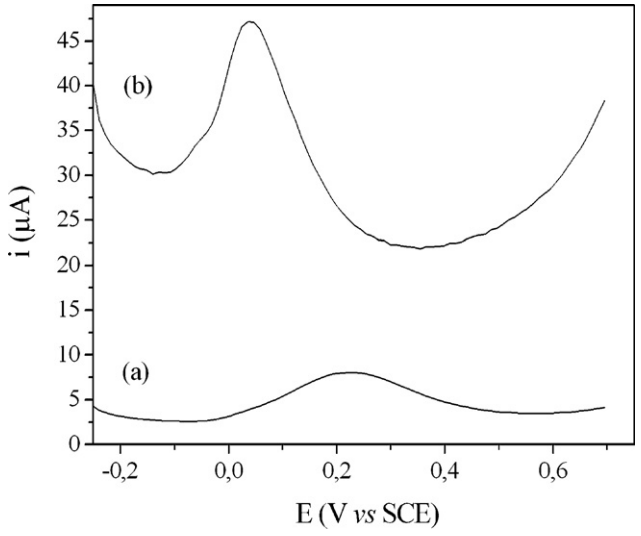

Fig. 5. Differential pulse voltammograms of 1.0×10^{-3} mol L^{-1} H_2AA, in pH 6.0 (buffer Tris–HCl) and 0.5 mol L^{-1} KCl solutions. Scan rate 10 mV s^{-1}. (a) The carbon–ceramic SiO_2/C electrode and (b) the SiO_2/C/Nb_2O_5 electrode.

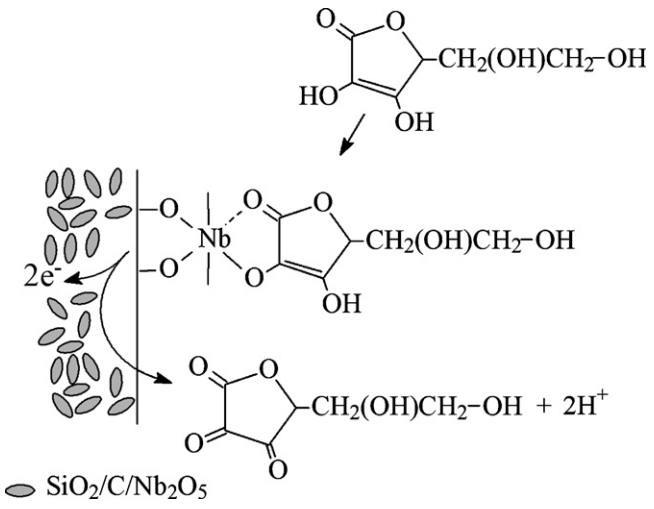

Scheme 2. Adsorption of ascorbic acid on the electrode surface and its oxidation.

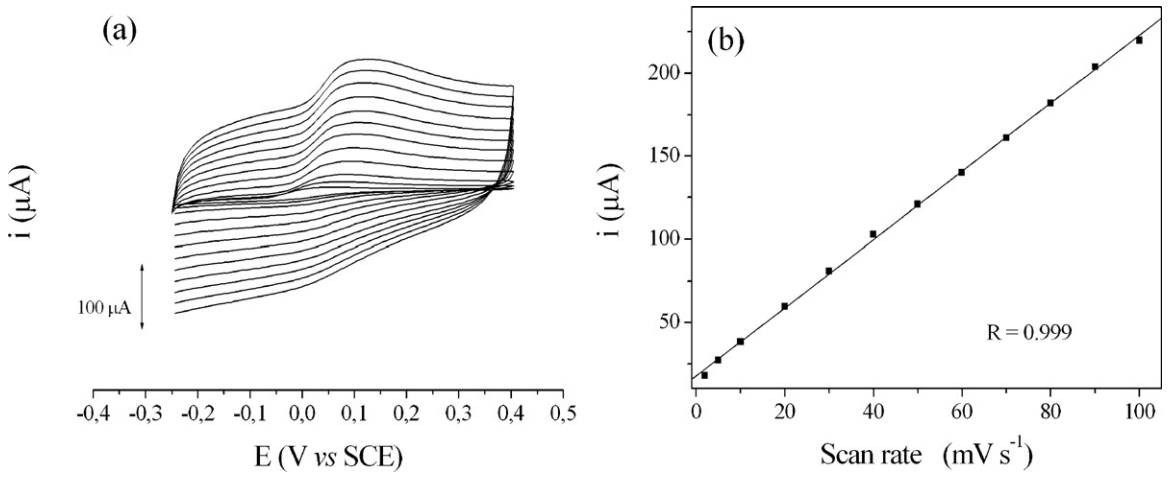

Fig. 6. Cyclic voltammograms obtained at different scan rates (2 at 100 mV s^{-1}) for $SiO_2/C/Nb_2O_5$ electrode (a), in 2.0×10^{-3} mol L^{-1} H_2AA, pH 6.0 (buffer Tris–HCl and 0.5 mol L^{-1} KCl). Relationship between peak current and scan rate (b).

theoretical expected value of 1.0 for an ideal case of the surface-adsorbed species with some contribution from diffusion [44].

The pH effects on the potential and current peaks were investigated by cyclic voltammetry (Fig. 7). The anodic peak of the H_2AA under different pH values shows potential shift to more negative values when the pH increases approximately from 3 to 5. Above this value, the potential remained constant. The anodic peak current intensity is not affected by the pH solution change in the pH range between 3 and 8. For practical applications we selected pH 7.0 to carry out the voltammetric determination of H_2AA.

In order to improve the sensitivity for the quantitative determination, DPV has been adopted to record the oxidation current of H_2AA at different concentrations. Fig. 8 shows the voltammograms from 0.0 to 2.38×10^{-3} mol L^{-1} of H_2AA acid in 0.5 mol L^{-1} KCl (0.1 mol L^{-1} Tris–HCl buffer, pH 7). In this range of ascorbic acid concentration, a linear correlation was observed (Fig. 8, inset), demonstrated by the equation $i\,(\mu A) = (23.76 \pm 0.10)[H_2AA]$ (mmol L^{-1}) with a linear correlation, $r = 0.999$ for $N = 16$. The achieved detection limit (3 standard deviation of the blank divided by the slope of calibration curve) was 25.03 μmol L^{-1} and sensitivity was 23.76 μA L $mmol^{-1}$. This result shows the potentiality of the $SiO_2/C/Nb_2O_5$ electrode to be utilized as an electrochemical sensor for ascorbic acid.

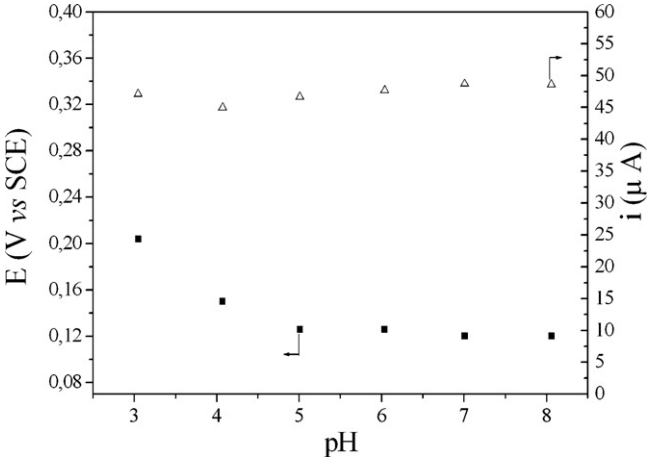

Fig. 7. Plots of the solution pH against E (■) and against i (△) for the $SiO_2/C/Nb_2O_5$ electrode, obtained by cyclic voltammetry, in 4.0×10^{-4} mol L^{-1} H_2AA in 0.5 mol L^{-1} of KCl with pH 3–8 solutions (The pH of the solution of H_2AA was set to the same pH as the KCl solution).

Table 2 shows some examples of the different electrodes for ascorbic acid determination. It can be seen that the $SiO_2/C/Nb_2O_5$ material is a competitive electrode for this analysis.

The $SiO_2/C/Nb_2O_5$ electrode presented good repeatability for ascorbic acid determinations. The relative standard deviation (RSD) of the peak current by DPV for 7 determinations in Tris–HCl buffer (pH 7.0) solution, containing 1.50×10^{-3} mol L^{-1} of the ascorbic acid, was 3.5%. A set of 3 sensors prepared in the same manner was also tested and the relative standard deviation observed was only 5.5%. Additionally, the electrode indicated prolonged operational and storage stability. When the electrode was stored in air and occasionally used over 9 months, the current response decreased by about 4%. These experiments indicate that the $SiO_2/C/Nb_2O_5$ electrodes have good stability and repeatability.

In the analysis of H_2AA, some coexistent electroactive species might affect the sensor response for example, dopamine (DA), uric acid (UA), paracetamol (PA), etc. These species should be considered because their oxidation peaks can overlap the H_2AA peak. Fig. 9

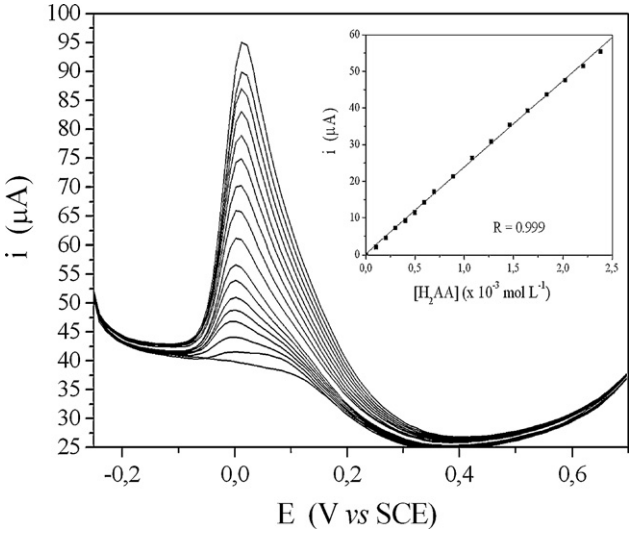

Fig. 8. Differential pulse voltammograms with $SiO_2/C/Nb_2O_5$ electrode, in 0.1 mol L^{-1} buffer Tris–HCl at pH 7 with 0.5 mol L^{-1} of KCl at scan rate 10 mV s^{-1}, containing different concentrations of H_2AA: 0.0, 9.98×10^{-5}, 1.99×10^{-4}, 2.98×10^{-4}, 3.97×10^{-4}, 4.95×10^{-4}, 5.93×10^{-4}, 6.90×10^{-4}, 8.84×10^{-3}, 1.08×10^{-3}, 1.27×10^{-3}, 1.46×10^{-3}, 1.64×10^{-3}, 1.83×10^{-3}, 2.02×10^{-3}, 2.20×10^{-3} and 2.38×10^{-3} mol L^{-1}. Inset shows the plot of the electrocatalytic peak current as a function of H_2AA concentration.

Table 2
Comparative performance of different electrodes for ascorbic acid determination.

Electrode	Method	Dynamic range (mmol L^{-1})	Limit of detection (μmol L^{-1})	Sensitivity (μA mmol^{-1} L)	Reference
CPE modified with copper(II) phosphate immobilized in a polyester resin	CV	0.02–3.2	10	–	[21]
GC modified with multiwalled carbon nanotubes grafted onto silica electro electrodeposited with gold nanoparticles	CV	1.0–5.0	–	8.59	[22]
Naphthol green B doped polypyrrole film	CV	0.24–25	110.00	7.3	[23]
CPE modified with polypyrrole/ferrocyanide films	CV	0.45–9.62	58.62	–	[24]
Gold modified with 3,4-dihydroxybenzoic acid and aniline	Amperometry	0.10–10.00	50	0.004	[25]
Graphite/propylpyridinium silsesquioxane	Amperometry	0.25–2.5	25	2.5	[26]
$SiO_2/C/Nb_2O_5$ material	PDV	0.099–2.38	25.03	23.76	This work

Table 3
Determination of ascorbic acid in commercial samples.

Commercial sample	Stated contents (g)	PDV method using the electrode (g)	Standard iodometric method (g)
Tablet A	1.0	0.999 (0.631)[a]	0.998 (0.492)
Tablet B	1.0	1.015 (0.871)	1.020 (0.590)

[a] RSD, % for $n = 4$.

shows the DPV responses of H_2AA, DA, UA, PA in pH 7.5 (Tris–HCl buffer). The oxidation of these species at the SiO_2/C electrode shows three broad overlapped anodic peaks (Fig. 9, curve b), suggesting that the oxidation peaks of DA, UA and PA are overlapped. Thus, DA, UA and PA could influence the oxidation signal of H_2AA at the unmodified SiO_2/C electrode. However, for $SiO_2/C/Nb_2O_5$ electrode, it was observed four separated peaks at −0.06 V, 0.11 V, 0.21 V and 0.31 V (Fig. 9, curve a). The oxidation peak potential difference between the species is about 100 mV, indicating that the species oxidations take place independently at the $SiO_2/C/Nb_2O_5$. Therefore, $SiO_2/C/Nb_2O_5$ is suitable for the selective detection of H_2AA.

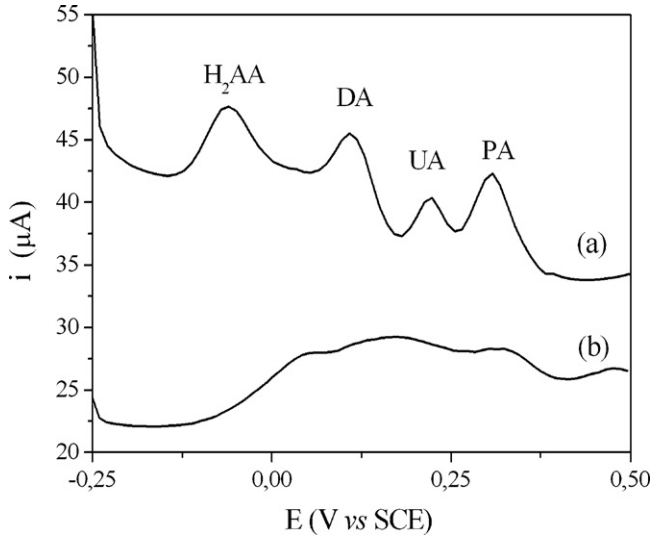

Fig. 9. DPV curves of 0.50 mmol L^{-1} H_2AA, 0.056 mmol L^{-1} DA, 0.20 mmol L^{-1} UA and 0.11 mmol L^{-1} PA in pH 7.5 buffer Tris–HCl. (a) $SiO_2/C/Nb_2O_5$ and (b) SiO_2/C.

3.3. Use of the $SiO_2/C/Nb_2O_5$ electrode to determine ascorbic acid in vitamin C tablets

In order to evaluate the applicability of this electrode for catalytic oxidation of H_2AA in real samples, effervescent tablets of vitamin C were examined by voltammetric determination of H_2AA. The results for these analyses with DPV, using $SiO_2/C/Nb_2O_5$ electrode, were compared to the standard iodometric method [45] and they are presented in Table 3. As can be observed, the obtained results are very close, showing that the electrode could be efficiently used for determination of ascorbic acid in commercial samples.

4. Conclusions

Nb_2O_5 was immobilized on the microporous carbon–ceramic matrix SiO_2/C. The Nb_2O_5 shows a homogeneous dispersion in micrometric level, and it improves the conductivity of the solid. The $SiO_2/C/Nb_2O_5$ material shows electrocatalytic activity in the oxidation of ascorbic acid and this property can be attributed to the interaction between Nb_2O_5 and ascorbic acid, forming a chemical bond and also due the semiconductor property of Nb_2O_5. This electrode showed stable, selective and reproducible response for ascorbic acid for several months, and it can be efficiently used for determination of ascorbic acid in commercial samples.

Acknowledgements

The authors thank FAPESP for fellowships L.T.A., process 06/61214-4 and financial support. They also thank the Brazilian Synchrotron Light Laboratory (LNLS) for the AFM/EFM measurements and are grateful to Prof. Carol H. Collins for manuscript review.

References

[1] R. Leitel, O. Stenzel, S. Wilbrandt, D. Gäbler, V. Janicki, N. Kaiser, Thin Solid Films 497 (2006) 135.
[2] F. Lai, M. Li, H. Wang, H. Hu, X. Wang, J.G. Hou, Y. Song, Y. Jiang, Thin Solid Films 488 (2005) 314.
[3] S. Martínez-Méndez, Y. Henríquez, O. Domínguez, L. D'Ornelas, H. Krentzien, J. Mol. Catal. A 252 (2006) 226.
[4] A.M. Gaffney, S. Chaturvedi, M.B. Clark Jr., S. Han, D. Le, S.A. Rykov, J.G. Chen, J. Catal. 229 (2005) 12.
[5] H. Miyake, H. Kozuka, J. Phys. Chem. B 109 (2005) 17951.
[6] K. Asakura, Y. Iwasawa, J. Phys. Chem. 95 (1991) 1711.
[7] M. Ziolek, Catal. Today 78 (2003) 47.
[8] D. Budziak, E.L. Silva, S.D. Campos, E. Carasek, Microchim. Acta 141 (2003) 169.
[9] M.S.P. Francisco, W.S. Cardoso, Y. Gushikem, Langmuir 20 (2004) 8707.
[10] C.A. Pessoa, Y. Gushikem, L.T. Kubota, Electrochim. Acta 46 (2001) 2499.
[11] C.A. Pessoa, Y. Gushikem, J. Porphyr. Phthalocya. 5 (2001) 537.
[12] S.S. Rosatto, P.T. Sotomayor, L.T. Kubota, Y. Gushikem, Electrochim. Acta 47 (2002) 4451.
[13] X. Xu, B. Tian, J. Kong, S. Zhang, B. Liu, D. Zhao, Adv. Mater. 15 (2003) 1932.
[14] X. Xu, B. Tian, S. Zhang, J. Kong, D. Zhao, B. Liu, Anal. Chim. Acta 519 (2004) 31.
[15] M. Tslonky, G. Gun, V. Glezer, O. Lev, Anal. Chem. 66 (1994) 1747.
[16] L. Rabinovich, O. Lev, Electroanalysis 13 (2001) 265.
[17] H. Razmi, E. Habibi, H. Heidari, Electrochim. Acta 53 (2008) 8178.
[18] G. Cabello-Carramolino, M.D. Petit-Dominguez, Microchim. Acta 164 (2009) 405.
[19] C.M. Maroneze, L.T. Arenas, R.C.S. Luz, E.V. Benvenutti, R. Landers, Y. Gushikem, Electrochim. Acta 53 (2008) 4167.
[20] A. Salimi, H. MamKhezri, R. Hallaj, Talanta 70 (2006) 823.
[21] M.F.S. Teixeira, L.A. Ramos, O. Fatibello-Filho, É.T.G. Cavalheiro, Anal. Bioanal. Chem. 376 (2003) 214.
[22] D. Ragupathy, A.I. Gopalan, K.P. Lee, Sens. Actuators B 143 (2010) 696.
[23] A. Mohadesi, M.A. Taher, Sens. Actuators B 123 (2007) 733.
[24] J.B. Raoof, R. Ojani, S. Rashid-Nadimi, Electrochim. Acta 49 (2004) 271.
[25] J.J. Sun, D.M. Zhou, H.Q. Fang, H.Y. Chen, Talanta 45 (1998) 851.
[26] R.V.S. Alfaya, Y. Gushikem, A.A.S. Alfaya, J. Braz. Chem. Soc. 11 (2000) 281.
[27] S. Denofre, Y. Gushikem, S.C. de Castro, Y. Kawano, J. Chem. Soc. Faraday Trans. 89 (1993) 1057.
[28] S. Brunauer, P.H. Emmett, E. Teller, J. Am. Chem. Soc. 60 (1938) 309.
[29] E.P. Barrett, L.G. Joyner, P.P. Halenda, J. Am. Chem. Soc. 73 (1951) 373.
[30] E.M. Girotto, I.A. Santos, Quim. Nova 25 (2002) 639.
[31] S.J. Gregg, K.S.W. Sing, Adsorption Surface Area Porosity, Academic Press, London, 1982 (Ch 3 and 4).
[32] J. Mulder, W.F. Stickle, P.E. Sobol, K.D. Bomben, Handbook of X-ray photoelectron Spectroscopy, Perkin-Elmer Corp., State of Minnesota, 1992.
[33] G. Speranza, L. Minati, M. Anderle, J. Appl. Phys. 102 (2007) 043504.
[34] H.K. Jeong, L. Colakerol, M.H. Jin, P.A. Glans, K.E. Smith, Y.H. Lee, Chem. Phys. Lett. 460 (2008) 499.
[35] H.K. Jeong, Y.P. Lee, R.J.W.E. Lahaye, M.H. Park, K.H. An, I.J. Kim, C.W. Yang, C.Y. Park, R.S. Ruoff, Y.H. Lee, J. Am. Chem. Soc. 130 (2008) 1362.
[36] M.S.P. Francisco, R. Landers, Y. Gushikem, J. Solid State Chem. 177 (2004) 2432.
[37] P. Carniti, A. Gervasini, M. Marzo, J. Phys. Chem. C 112 (2008) 14064.
[38] K.H.A. Bogart, V.M. Donnelly, J. Appl. Phys. 87 (2000) 8351.
[39] V. Boffa, J.E. ten Elshof, R. Garcia, D.H.A. Blank, Micropor. Mesopor. Mater. 118 (2009) 202.
[40] J. Argüello, V.L. Leidens, H.A. Magosso, R.R. Ramos, Y. Gushikem, Electrochim. Acta 54 (2008) 560.
[41] S. Denofre, Y. Gushikem, C.U. Davanzo, Eur. J. Solid State Inorg. Chem. 28 (1991) 1295.
[42] M.A. Aegerter, Sol. Energy Mater. Sol. Cell 68 (2001) 401.
[43] U. Chandra, B.E.K. Swamy, O. Gilbert, B.S. Sherigara, Electrochim. Acta 55 (2010) 7166.
[44] A.J. Bard, L.R. Faulkner, Electrochemical Methods: Fundaments Applications, John Wiley, New York, 1980.
[45] O. Zenebon, N.S. Pascuet, Métodos Físico-Químicos para Análise de Alimentos, Instituto Adolfo Lutz, Brasília, 2005, p. 169.